Journal of Bacteriology

Mutational and Structural Analysis of l-*N*-Carbamoylase Reveals New Insights into a Peptidase M20/M25/M40 Family Member

Sergio Martínez-Rodríguez, Abel García-Pino, Francisco Javier Las Heras-Vázquez, Josefa María Clemente-Jiménez, Felipe Rodríguez-Vico, Juan M. García-Ruiz, Remy Loris and Jose Antonio Gavira

J. Bacteriol. **2012, 194(21):5759. DOI: 10.1128/JB.01056-12. Published Ahead of Print 17 August 2012.**

Updated information and services can be found at:
http://jb.asm.org/content/194/21/5759

These include:

SUPPLEMENTAL MATERIAL Supplemental material

REFERENCES This article cites 56 articles, 15 of which can be accessed free at: http://jb.asm.org/content/194/21/5759#ref-list-1

CONTENT ALERTS Receive: RSS Feeds, eTOCs, free email alerts (when new articles cite this article), more»

Information about commercial reprint orders: **http://journals.asm.org/site/misc/reprints.xhtml**
To subscribe to to another ASM Journal go to: **http://journals.asm.org/site/subscriptions/**

Journals.ASM.org

Downloaded from http://jb.asm.org/ on October 8, 2012 by guest

JB
Journals.ASM.org

Mutational and Structural Analysis of L-*N*-Carbamoylase Reveals New Insights into a Peptidase M20/M25/M40 Family Member

Sergio Martínez-Rodríguez,[a] Abel García-Pino,[b] Francisco Javier Las Heras-Vázquez,[a] Josefa María Clemente-Jiménez,[a] Felipe Rodríguez-Vico,[a] Juan M. García-Ruiz,[c] Remy Loris,[b] and Jose Antonio Gavira[c]

Departamento de Química Física, Bioquímica y Química Inorgánica, Universidad de Almería, Almería, Spain[a]; Molecular Recognition Unit, Structural Biology Brussels, Vrije Universiteit Brussel, and Department of Molecular and Cellular Interactions, Vlaams Interuniversitair Instituut voor Biotechnologie, Brussels, Belgium[b]; and Laboratorio de Estudios Cristalográficos, Instituto Andaluz de Ciencias de la Tierra (CSIC-UGR), Granada, Spain[c]

***N*-Carbamoyl-L-amino acid amidohydrolases (L-carbamoylases) are important industrial enzymes used in kinetic resolution of racemic mixtures of *N*-carbamoyl-amino acids due to their strict enantiospecificity. In this work, we report the first L-carbamoylase structure belonging to *Geobacillus stearothermophilus* CECT43 (BsLcar), at a resolution of 2.7 Å. Structural analysis of BsLcar and several members of the peptidase M20/M25/M40 family confirmed the expected conserved residues at the active site in this family, and site-directed mutagenesis revealed their relevance to substrate binding. We also found an unexpectedly conserved arginine residue (Arg^{234} in BsLcar), proven to be critical for dimerization of the enzyme. The mutation of this sole residue resulted in a total loss of activity and prevented the formation of the dimer in BsLcar. Comparative studies revealed that the dimerization domain of the peptidase M20/M25/M40 family is a "small-molecule binding domain," allowing further evolutionary considerations for this enzyme family.**

N-Carbamoyl-L-amino acid amidohydrolases (L-carbamoylases; EC 3.5.1.87) irreversibly hydrolyze the amide bond of the carbamoyl group in L-*N*-carbamoyl-amino acids. Due to their stereospecificity, L-carbamoylases are widely used in kinetic resolution for the production of optically pure amino acids (see reference 44 and references therein). Furthermore, their substrate promiscuity allows their use in different multienzymatic processes, increasing their economic and industrial relevance (48). L-Carbamoylases have been isolated and characterized from different sources, although most of the studies carried out have focused on biotechnological applications (44). Their relationship with other amidohydrolases and with the peptidase M20/M25/M40 family has been established based on sequence similarity (21, 29, 42). A closer relationship among L-carbamoylases and β-ureidopropionases is supported by the findings of two β-ureidopropionases that are able to hydrolyze *N*-carbamoyl-L-α-amino acids (40, 41, 47).

In a previous work, we were able to show the involvement in catalysis of several highly conserved residues in L-carbamoylases, as well as the relationship of these enzymes with several peptidases (42). Dimerization was also proved to be necessary for enzymatic activity, as the residues involved in catalysis come from both monomers. In this work, we determined the first crystal structure of an L-carbamoylase, belonging to *Geobacillus stearothermophilus* CECT43 (BsLcar). Mutagenesis studies of BsLcar confirmed the importance of conserved residues in this enzyme. Unexpectedly, a highly conserved arginine in L-carbamoylases has been proved critical for the dimerization of the enzyme, and thus for enzymatic activity. Comparative studies revealed striking characteristics of the different "dimerization" domains of the peptidase M20/M25/M40 family, in agreement with previous evolutionary hypotheses on this family of enzymes (3, 37) and suggesting new evolutionary considerations. Finally, an alternative reaction mechanism dependent on only one metal atom can be inferred from the experimental data.

MATERIALS AND METHODS

Structure determination and refinement. The procedures for the purification, crystallization, and data collection of BsLcar are described in detail elsewhere (43). Briefly, purified BsLcar was dialyzed against 20 mM Tris, pH 8.0, and crystallization conditions were determined using Hampton Research crystal screens I and II. The best-diffracting crystals were obtained in 20% 2-propanol, 0.1 M HEPES, pH 7.5, 0.2 M trisodium citrate at 293 K. Data were collected from a single crystal on a Bruker AXS Microstar Proteum machine and processed using the Proteum software suite (Bruker AXS Inc.). Molecular replacement was carried out with MOLREP (56), using two isolated domains of allantoate amidohydrolase from *Escherichia coli* (EcAam; Protein Data Bank [PDB] ID 1Z2L; 35% sequence similarity) (2, 43). After initial simulated annealing with phenix.refine (1), restrained positional refinement was carried out with the program REFMAC5 (45) from the CCP4 software suite (Collaborative Computational Project Number 4 software for macromolecular X-ray crystallography), using a test set of 5% of the total reflections to calculate R_{free}. Coot (16) was used for visualization and manual rebuilding of protein; water molecules and heteroatoms were added manually with the same program. After refinement and previous deposition in the Protein Data Bank, the quality of the model was checked using MolProbity (13). Refinement parameters and statistics of the final model of BsLcar are summarized in Table 1.

Recloning of the BsLcar gene into the pJOE4036.1 plasmid and site-directed mutagenesis. Recloning of the *Bslcar* gene into plasmid pJOE4036.1 (54) was performed because this plasmid has been proved to improve the overexpression of other carbamoylase enzymes in our lab

Received 14 June 2012 Accepted 9 August 2012
Published ahead of print 17 August 2012
Address correspondence to Sergio Martínez-Rodríguez, srodrig@ual.es.
S.M.-R. and A.G.-P. contributed equally to this work and are considered co-first authors.
Supplemental material for this article may be found at http://jb.asm.org/.
Copyright © 2012, American Society for Microbiology. All Rights Reserved.
doi:10.1128/JB.01056-12

Downloaded from http://jb.asm.org/ on October 8, 2012 by guest

TABLE 1 Data collection and refinement statistics for BsLcar[b]

Statistic	Value or description
Data collection statistics	
Wavelength (Å)	1.54
Temperature (K)	100
Space group	P21212
a, *b*, *c* distances (Å)	103.2, 211.7, 43.1
Matthews coefficient ($Å^3$ Da^{-1})	2.67
No. of monomers per asymmetric unit	2
Resolution (Å)	20.0–2.75
No. of observed reflections	23,771
Redundancy	7.26 (3.92)
Completeness (%)	98.5 (91.5)
R_{sym} (%)[a]	12.4 (25.8)
Average I/σ (I)	15.1 (4.2)
Refinement statistics	
R value (%)	19.3 (23.4)
R_{free} value (%)	27.6 (31.7)
No. of reflections in working set	1,495
No. of solvent molecules	128
No. of heteroatoms	2 Co^{2+}, 1 cacodylate, 2 isopropanol
Average B factor ($Å^2$)	14.70
RMSD bond length (Å)	0.014
RMSD bond angle (°)	1.556
Ramachandran plot statistics	
Most favored regions (%)	93.3
Allowed regions (%)	0.1
Generally allowed regions (%)	6.4
Disallowed regions (%)	0.1
Residues in disallowed regions	Ser78A, Ser78B

[a] $R_{sym} = \Sigma_h\Sigma_i|[I_i(h) - \langle I(h)\rangle]|/\Sigma_h\Sigma_i I_i(h)$, where $I_i(h)$ is the ith measurement of reflection h and $\langle I(h)\rangle$ is the weighted mean of all measurements of h.
[b] Statistical values for the highest-resolution shell (2.85 to 2.75 Å) are given in parentheses.

(data not shown). The plasmid pJAVI80 (43) was used as the donor template for PCR. The PCR products and the vector pJOE4036.1 were digested with NdeI and BamHI enzymes, gel purified, and ligated to create pJAVI80rha, allowing overexpression of BsLcar fused to a His_6 tag at its C terminus. Mutagenesis of BsLcar His^{225}, Arg^{234}, Thr^{261}, Asn^{273}, Asp^{284}, and Arg^{286} was performed using a QuikChange II site-directed mutagenesis kit from Stratagene following the manufacturer's protocol, using pJAVI80rha plasmid as the template. The cloned sequence and mutations were confirmed by sequencing in an ABI 377 DNA sequencer (Applied Biosystems).

Expression of constructs and purification of resulting enzymes. *E. coli* BL21/pJAVI80rha and the mutated strains were grown in LB medium supplemented with 100 μg ml^{-1} of ampicillin. A single colony was transferred into 10 ml of LB medium with ampicillin at the above-mentioned concentration. This culture was incubated overnight at 37°C with shaking. One thousand milliliters of LB medium with the appropriate concentration of ampicillin was inoculated with 10 ml of the overnight culture. After 3 to 4 h of incubation at 37°C with vigorous shaking, the optical density at 600 nm (OD_{600}) of the resulting culture was 0.3 to 0.5. For induction of expression of the genes, L-rhamnose was added to a final concentration of 0.2% (wt/vol) and the culture was incubated at 32°C overnight. The cells were collected by centrifugation (Beckman JA2-21 centrifuge) (7,000 × *g*, 4°C, 15 min) and stored at −20°C until use.

Procedures for the purification and preparation of the wild-type and mutated enzymes by cobalt affinity chromatography were performed as described above. After purification, gel filtration chromatography was carried out using a Superdex 200 gel filtration column (GE Healthcare) in a BioLogic DuoFlow fast-performance liquid chromatography (FPLC) system (Bio-Rad) to eliminate any DNA or protein coeluting with the protein of interest. The purified enzymes were concentrated using Vivaspin concentrators (Sartorius), dialyzed against the optimum buffer, described previously (0.1 M sodium phosphate, pH 7.5) (48), and stored at 4°C until use. Protein concentrations were determined from the absorbance of extinction coefficient of tyrosine residues (19). SDS-PAGE and native PAGE were used to determine the purity and aggregation state of the recombinant proteins.

Molecular mass analysis. Size-exclusion chromatography–high-pressure liquid chromatography (SEC-HPLC) analysis was performed to calculate the molecular masses of the different mutants, using a nondenatured protein molecular size marker kit (Sigma-Aldrich). An HPLC system (LC2000Plus HPLC system; Jasco) equipped with a BioSep-SEC-S2000 column (Phenomenex) was equilibrated and eluted with 0.1 M sodium phosphate buffer, pH 7.5, at a flow rate of 0.5 ml min^{-1}, and then the absorbance at 280 nm was measured.

Static light scattering (SLS) measurements were carried out with wild-type and R234A mutant BsLcar samples on a Zetasizer Nano ZS instrument (Malvern), using a thermostatized 12-μl quartz cuvette (25°C). The average scattering intensities for five different concentrations (1 to 5 mg/ml in 0.1 M sodium phosphate buffer, pH 7.5) were recorded. Solutions were filtered and centrifuged for 30 min at 14,000 rpm immediately prior to measurement in order to remove aggregates and dust. The integrated control software developed by Malvern Instruments Ltd. was run to collect, process, and analyze the data. Molecular masses of the molecules were determined using a Debye plot, which allows the determination of both absolute molecular mass (M) and the second virial coefficient (A_2), using the following equation:

$$\frac{KC}{R_0} = \left(\frac{1}{M} + 2A_2C\right) \quad (1)$$

where K is an optical constant, R_0 is the Rayleigh ratio of the scattered to incident light intensity, and C is the sample concentration (57; Malvern Zetasizer Nano application note MRK577-01).

Circular dichroism experiments. The secondary structures of wild-type and mutated BsLcar were compared using far-UV circular dichroism (CD) spectra, recorded with a Jasco J810 CD spectrometer equipped with a Jasco PTC-423S/15 Peltier accessory. The protein concentration was 1.5 μM in 1 mM sodium phosphate buffer, pH 7.5. CD measurements were taken at 25°C, using a 0.1-mm-path-length cuvette. Spectra were acquired from 250 to 190 nm, at a scan rate of 50 nm min^{-1}. For each protein, a baseline scan (buffer) was subtracted from the average of six scans to give the final averaged scan.

Enzyme assay and protein characterization. To assess whether cobalt was the cation present in the catalytic center, we carried out (i) spectrophotometric complexation with 4-(2-pyridylazo)resorcinol (50) and (ii) inductively coupled plasma mass spectrometry (ICP-MS) on liquid protein samples treated with aqua regia (10% [vol/vol]). ICP-MS was also carried out on dissolved crystals. Two drops containing several crystals was centrifuged in an Eppendorf tube, washed carefully with 5 μl of cold water, and dissolved in aqua regia (10% [vol/vol]). Blanks (prepared using the solution used for crystallization) and a solution containing egg white lysozyme were used as negative controls. Samples were injected into an ICP-MS instrument (X series 2 ICP-MS; Thermo Fisher) at the University of Almería's central research services.

A standard enzymatic reaction was carried out with BsLcar and mutated enzymes, using a slightly modified method compared to that previously described (48). One hundred microliters of 5 μM enzyme solution was preincubated with 1 mM $CoCl_2$ for 1 h. Four hundred microliters of 10 mM *N*-carbamoyl-L-methionine in 0.1 M sodium phosphate buffer (pH 7.5) was added and incubated at 50°C. Aliquots (75 μl) were removed at 5, 10, and 15 min, and the reaction was stopped by addition of 675 μl of 1% H_3PO_4. After centrifugation, the supernatant was analyzed by HPLC.

Downloaded from http://jb.asm.org/ on October 8, 2012 by guest

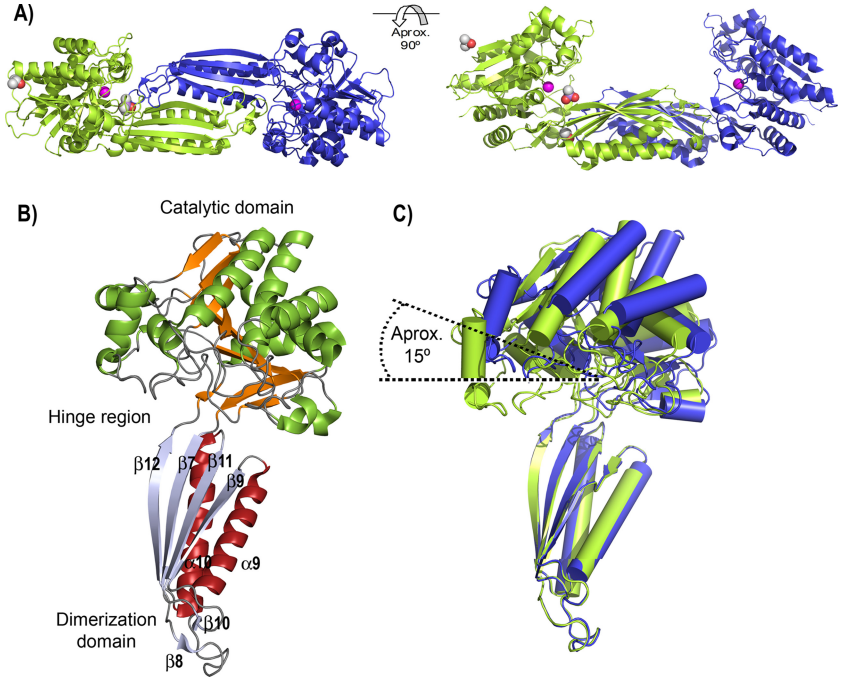

FIG 1 (A) Dimeric arrangement of BsLcar showing the positions of the cobalt cations (magenta) and the isopropanol and cacodylate molecules (red and white). (B) Domain architecture of monomeric BsLcar, showing the α/β/α sandwich catalytic domain (green and orange) connected through the hinge region to the βαββαβ dimerization domain (red and purple). Secondary structure elements not shown by Pymol (β8 and β10) but calculated by PROMOTIF (30) through the PDBsum server (34) were inserted manually. (C) Superposition of BsLcar chains A and B, showing the differences produced by domain motion.

The HPLC system described above, equipped with a Luna C_{18} column (4.6 × 250 mm; Phenomenex), was used to detect the product and substrate of the reaction. The mobile phase was 90% phosphoric acid (20 mM, pH 3.2) and 10% methanol, pumped at a flow rate of 0.75 ml min^{-1} and measured at 210 nm.

Analysis of BsLcar structure. The Dali server (26) was used to search for folds similar to that presented by the BsLcar structure. The PISA and PDBsum servers (33, 34) were used to analyze the interfaces and secondary structure of BsLcar. Swiss-PDB Viewer (23) was used for manual manipulation/comparison of the structures. Pymol (http://www.pymol.org) and Coot (16) were used for generation of graphics.

Protein structure accession number. Coordinates and structure factors for BsLcar have been deposited at the RCSB PDB under entry code 3N5F.

RESULTS AND DISCUSSION

Overall structure of BsLcar. The asymmetric unit of BsLcar contains two polypeptide chains, A and B, comprising residues Gln^3 to Gly^{408} for both chains A and B (Fig. 1A). BsLcar proved to be a homodimer in solution by gel filtration chromatography (43), as expected for L-carbamoylases (44), since dimerization is essential for their activity. Thus, the arrangement observed in the asymmetric unit likely corresponds to that observed in solution. The BsLcar fold is composed of two domains (Fig. 1B), reminiscent of the peptidase M20/M25/M40 family (the counterpart of the M20 family in the MEROPS peptidase database) (Table 2). Following the nomenclature used for several enzymes of the family, we identified two domains, known as the "catalytic" and "dimerization" (or "lid") domains. The catalytic domain of L-carbamoylase comprises residues 1 to 207 and 326 to 409, whereas the inserted 118-residue fragment constitutes the dimerization domain (residues 208 to 325). A linker region referred to as the "hinge region" connects both domains.

Superposition of both monomers of BsLcar did not result in structurally identical polypeptide chains (Fig. 1C), showing a global root mean square deviation (RMSD) of 2.37 Å for 406 common α-carbon atomic pairs. On the other hand, superposition of the isolated catalytic and dimerization domains resulted in RMSD of 0.64 Å and 0.42 Å for the 288 and 118 common α-carbon atomic pairs, respectively. This difference arises from an approximation of the catalytic domain toward the dimerization domain of chain B, with a difference of approximately 15° with respect to chain A (Fig. 1C). This domain movement likely arises from the presence of a molecule bound in the cleft formed between the catalytic and dimerization domains. Crystal packing also gives support to this arrangement. In this sense, the same open-and-closed conformation was observed for allantoate amidohydrolase (PDB ID 1Z2L), for which it was already proposed that this conformation was stabilized by the crystallization process (2). Analysis of the electron density maps together with the crystallization conditions used suggests that this molecule is a cacodylate (see Fig. S1 in the supplemental material).

The dimerization domain (residues 208 to 325) is formed by a long four-stranded antiparallel β-sheet (β9-β11-β7-β12) accompanied by two long α-helices on one side of the β-sheet (α9-α10) and a small inserted antiparallel β-sheet (β8-β10) (Fig. 1B). Without the small β8-β10 strands, this domain forms a βαββαβ topology showing a predominant nonpolar core. The four-stranded β-sheet belonging to one monomer continues in the adjacent one, forming an extended eight-stranded antiparallel β-sheet (Fig. 1A and 2A). The contact interface of dimeric BsLcar consists of 43 and 45 residues from chains A and B, respectively. The majority of the interface comes from 16 direct hydrogen bonds plus 191 van der Waals contacts that cover an area of approximately 2,175 $Å^2$. The

Downloaded from http://jb.asm.org/ on October 8, 2012 by guest

TABLE 2 Characteristics of homologous enzymes of BsLcar obtained using the Dali server[a]

Enzyme	PDB ID	Chain	*Z* value	% Identity	RMSD (Å)	Residue(s)								
						Metal 1		Bridge	Metal 2		Base	Binding		
BsLcar	3N5F	A				H79	H189	D90	E125	H380	E124	R286	H225(B)	N273(B)
Allantoate amidohydrolase (EcAam)	1Z2L	A	47.4	34	2.4	H83	H192	D94	E129	H384	E128	R290	H228(B)	N277(B)
β-Ureidopropionase (Skβas)	1R3N	G	46.9	33	2.9	H114	H226	D125	E160	H421	E159	R322	H262(B)	N309(B)
Peptidase T (NP)[b]	3GB0	A	30.0	25	4.5	H77	D164	D107	E141	H345	E140	R250	H192(B)	N237(B)
Carboxypeptidase G2 (CPG2)	1CG2	A	28.8	20	5.9	H112	E200	D141	E176	H385	E175	R288	H229(B)	N275(B)
Succinyl-diaminopimelate desuccinylase	1VGY	A	28.6	16	3.9	H68	E164	D101	E136	H350	E135	R259	H195(B)	N246(B)
Protein YXEP (NP)	1YSJ	A	27.6	19	4.8	H100	H158	C98	E134	H350	E133	R254	H192(B)[c]	N241(B)
Peptidase T	1VIX	A	27.4	16	4.8	H78	D196	D140	E174	H379	E173	R280	H223(B)	
Peptidase T[b]	1FNO	A	27.2	16	5	H78	D196	D140	E174	H379	E173	R280	H223(B)	
IAA-amino acid hydrolase homolog 2 (ILL2)	1XMB	A	27.1	18	5.4	H139	H197	C137	E173	H397	E172	R293	H231(B)[c]	N280(B)[c]
Succinyl-diaminopimelate desuccinylase (DapE)	3IC1	A	26.9	15	6.3	H67	E163	D100	E135	H349	E134	R258	H194(B)[c]	N244(B)[c,d]
Peptidase T (NP)[b]	3IFE	A	26.6	17	4.4	H79	D199	D142	E177	H381	E176	R283	H226(B)	
Acetylornithine deacetylase (NP)	3PFO	A	26.1	15	6.3	H110	E201	D143	E178	H401	E177	R297	H227(B)	S286(B)[e]
Cocatalytic metallopeptidase (NP)	2RB7	B	25.4	14	5.5	H72	D162	D99	E139	H332	E138	R251	H189(B)	N238(B)
Acetylornithine deacetylase (NP)	3CT9	B	23.9	17	4.9	H73	E161	D104	E137	H328	E136	R249	H187(B)[f]	N236(B)
Aminobenzoyl-glutamate utilization protein (NP)[g]	3IO1	A	23.6	13	7.6	H151	H209	C149	E184	H406	E183	R301	H241(B)	N288(B)
Peptidase V (PepV)	1LFW	A	23.0	14	5.2	H87	D177	D119	E154	H439	E153	R350	H269(A)	N217(A)
Carnosine dipeptidase (NP)	3DLJ	A	22.7	17	6.1	H106	D202	D139	E174	H452	E173	R350	H235(B)	T337(B)[e]
Metallopeptidase (Sapep)	3KI9	A	22.0	12	5.9	H84	D173	D115	E150	H440	E149	R350	H269(A)	N216(A)
Carnosinase	2ZOG	A	22.0	15	6.6	H99	D195	D132	E167	H445	E166	R343	H228(B)	T330(B)[e]
Xaa-His dipeptidase (NP)	2QYV	A	21.8	17	6.7	H76	D169	D115	E145	H458	E146	R366	H214(A)	N258(A)
Acetylcitrulline deacetylase (ACDase)[b]	2F8H	A	21.7	15	5.3	H72	E155	D103	E131	H340	E130	R248	H181(B)[c]	N235(B)
Metallopeptidase (NP)	2POK	A	21.6	11	5	H90	E184	D123	E158	H431	E157	R334	H218(B)	T321(B)[e]
Metallopeptidase (NP)	3PFE	A	21.5	16	5.3	H96	D190	D129	E163	H442	E162	R340	H223(B)	N327(B)
Aminoacyl histidine dipeptidase (PepD)	3MRU	A	19.9	16	5	H80	D173	D119	E150[h]	H461	E149[h]	R369	H219(A)	N260(A)

[a] The counterpart residues of the conserved bimetallic center and the binding residues of BsLcar are shown. RMSD was measured for the whole chain. In the "binding residues" columns, "(A)" indicates that the residues belong to the same monomer as the Arg residue, and "(B)" indicates that they belong to the second monomer of the dimer. NP, nonpublished results (only the PDB ID is available).

[b] Dimeric arrangement was generated by symmetry.

[c] Loops containing these residues do not appear in the corresponding PDB structures and have been assigned based on their primary sequence.

[d] This Asn residue appears in only one chain, and the loop where it appears is displaced with respect to the rest of the structures.

[e] Residues spatially situated where the Asn residue would be located.

[f] This His residue appears a little further away in space than the rest of the structures, most probably due to binding to chloride and iodide ions in this zone.

[g] This structure presents several unmodeled blobs, among them zones including important residues, and the numeration of the residues was obtained by sequence alignment with the structures under PDB IDs 1YSJ and 1XMB.

[h] Numeration was retrieved from reference 9. However, Glu^{149} is closer to M2 than Glu^{150}.

residues involved in this interface are predominantly part of the dimerization domain and interact by helix-helix interactions (α9A-α9B, with a marked hydrophobic character) and by multiple contacts between the segments comprising β8A-α9A and β9B-β11B. Sequence alignment of BsLcar with 501 protein sequences with over 50% similarity, retrieved from a BLAST search using the Uniprot database (data not shown), shows a low conservation of the residues involved in the interface. Only the R^{234A}-T^{261B} pair (Fig. 2A and B; also see Fig. S2 in the supplemental material) is highly conserved within all compared sequences (100 and 95% similarity for R^{234} and T^{261}, respectively).

Roles of highly conserved residues in activity and oligomerization of BsLcar. In order to evaluate the involvement of several residues that are highly conserved in L-carbamoylases (see Fig. S2 in the supplemental material), six mutants were created: the H225A, R234A, T261A, N273A, D284E, and R286A mutants. Far-UV CD spectra were collected to evaluate the correct folding of all of them (see Fig. S3). No significant differences were found, suggesting that the α-plus-β structure was not changed in the mutants, and thus they did not significantly alter BsLcar folding. Table 3 shows the relative activities of wild-type and mutated BsLcar species, confirming the importance of these residues in the

Downloaded from http://jb.asm.org/ on October 8, 2012 by guest

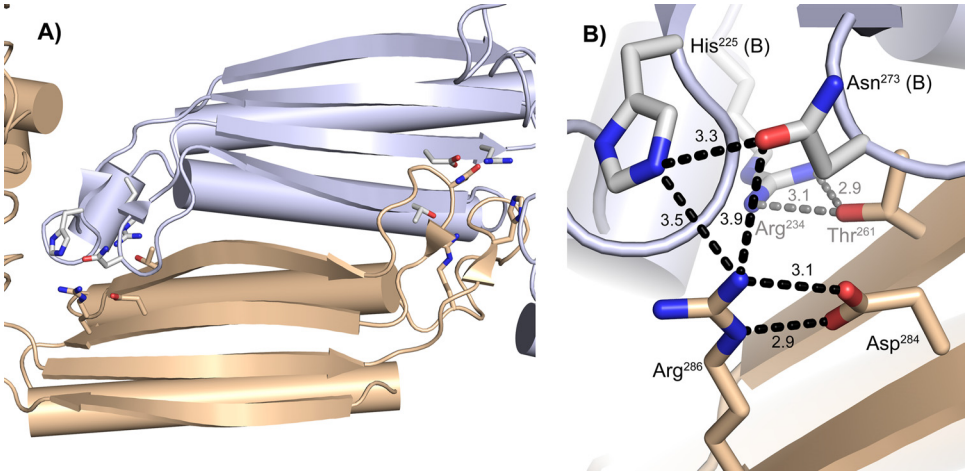

FIG 2 (A) Extended eight-stranded antiparallel β-sheet formed by dimerization of BsLcar chains A (gold) and B (purple). The relative positions of the binding residues Arg^{286}, His^{225}, and Asn^{273} and the newly identified important residues for L-carbamoylases (Arg^{234}, Thr^{261}, and Asp^{284}) are shown. (B) Close-up view of the same residues showing environmental distances (colors are the same as in panel A).

activity of the enzyme. The quaternary structure was determined by means of SEC-HPLC, native PAGE, and SLS techniques. With a BioSep-SEC-S2000 column, all of the mutants showed the same retention time as wild-type BsLcar, except for the R234A mutant, which showed a longer retention time and an estimated molecular mass of 44 kDa (Fig. 3A). The same behavior was observed by blue native PAGE analysis, in which the R234A mutant migrated faster, suggesting a monomeric species (Fig. 3A, inset). SLS experiments carried out with the wild type and the R234A mutant rendered molecular mass values of 120.6 and 73.6 kDa, respectively. The theoretical values for dimeric and monomeric species of BsLcar are 90 and 45 kDa, respectively, which differ considerably from the values obtained experimentally by SLS. On the other hand, an approximately 2:1 ratio is maintained between the values obtained for the wild-type and R234A species. The discrepancies between the experimental and theoretical values are most likely due to the assumption of a globular form for assignment of the differential refractive index increment (dn/dC) contained in the optical constant K in equation 1, whereas BsLcar dimers and monomers present an elongated shape (Fig. 1A and B). Taken as a whole, the results indicate that the dimeric arrangement of BsLcar is disrupted in the R234A mutant, and this is also supported by the total loss of activity (Table 3). Since Thr^{261} mutation did not disrupt the dimer, it seems clear that the hydrogen bond between Arg^{234} and Thr^{261} is not the only oligomerization-driving force in BsLcar (Fig. 3B). Structural analysis of this region showed several other inter- and intrachain interactions of Arg^{234}; in particular, Arg^{234A}, Met^{231A}, and Gly^{260B} are highly coordinated (Fig. 3B). Arg^{234A} further seems to assist in correct positioning of the preceding Glu^{224A}-Pro^{230A} loop via Ala^{226A} and Thr^{229A}, where His^{225} is situated (see the importance of this residue below). Thus, mutation of Arg^{234} alters this extensive bonding network, which as a whole seems to be necessary for dimerization.

TABLE 3 Relative activities of wild-type and mutated BsLcar species toward *N*-carbamoyl-L-methionine

BsLcar species	Relative activity (%)
Wild type	100 ± 5
R286A mutant	ND[a]
H225A mutant	ND
N273A mutant	6 ± 2
D284E mutant	6 ± 3
R234A mutant	ND
T261A mutant	25 ± 10

[a] ND, not detected.

The active site: are two metal ions indispensable for enzymatic activity? L-Carbamoylases were previously shown to present a binuclear metal center common to other members of the peptidase M20/M25/M40 family and to several peptidases composed only of the catalytic domain (38, 42) (these are grouped under the MEROPS peptidase M28 family and are henceforth referred to as cc-peptidases). BsLcar activity increases by factors of 3 and 7 with the addition of Mn^{2+} and Co^{2+}, respectively, whereas Zn^{2+} does not have a significant effect (48) (compared to the nonamended purified enzyme). Although initial inspections of the BsLcar |Fo-Fc| electron density maps showed two peaks at the active site of chain B (43), only one metal atom could be fitted at full occupancy during the refinement process. This result is not surprising, as no divalent metal was included during the crystallization experiments and a lack or half-occupancy of cations in this conserved bimetallic center has been observed in analog structures (e.g., PDB IDs 1VGY, 1XMB, 2F7V, 2FH8, 2IMO, 2POK, 2RB7, 3CT9, and 3GB0). Cobalt was chosen as the metal in the BsLcar structure, based on the recorded spectra of protein samples treated with 4-(2-pyridylazo)resorcinol (50). Liquid BsLcar samples (0.06 μmol monomeric species) were also analyzed by ICP-MS, giving 301 ± 3 ppb of Co^{2+} (0.05 μmol), resulting in a ratio of 0.8 atom of Co^{2+} per monomer of BsLcar. Although we could not estimate the ratio of metal bound in the dissolved BsLcar crystals, its presence was further confirmed by ICP-MS (5 ± 1 ppb). We suspect that Co^{2+} is incorporated during the purification process.

The most accepted reaction mechanism for several members of the peptidase M20/M25/M40 family involves a water molecule bridged by the two metal ions which is activated by a conserved general base (Table 2), thus allowing the nucleophilic attack of the amide bond of the substrates (7, 9, 31, 36–38, 46, 49, 55). This

Downloaded from http://jb.asm.org/ on October 8, 2012 by guest

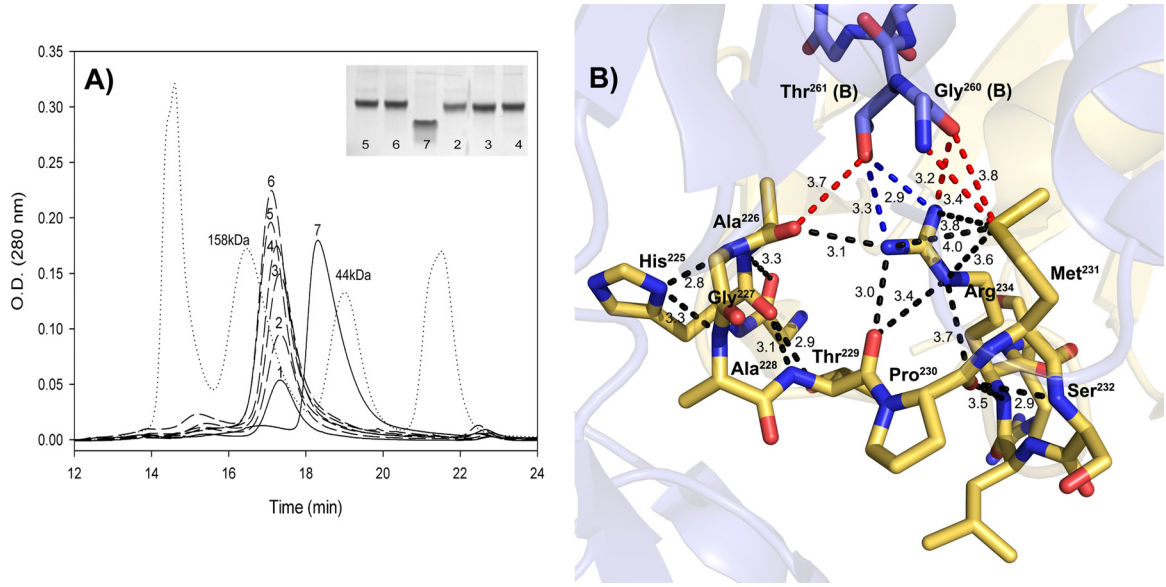

FIG 3 (A) SEC-HPLC analysis of the purified wild-type and mutated BsLcar species and of a gel filtration standard (Bio-Rad) (dotted line). The peaks corresponding to the gel filtration standard are as follows: for thyroglobulin, 670 kDa; for bovine gamma-globulin, 158 kDa; for chicken ovalbumin, 44 kDa; and for equine myoglobin, 17 kDa. Data for wild-type BsLcar (line 1) and the R234A mutant (line 7) appear as solid lines, whereas data for the rest of the mutants (lines 2 to 6) appear as dashed lines. Numeration is as follows: 1, wild-type BsLcar; 2, H225A mutant; 3, N273A mutant; 4, R286A mutant; 5, D284E mutant; 6, T261A mutant; and 7, R234A mutant. The inset corresponds to native PAGE analysis of mutated species, following the same numeration as in the SEC-HPLC analysis. (B) Interactions found in the Arg^{234}-Thr^{261} environment. The hydrogen bond between both residues appears in blue, whereas other inter- and intrachain interactions are represented in red and black, respectively.

mechanism is based on homology with cc-peptidases, in which the bimetallic center is also conserved (27). On the other hand, the metal ions have been associated with different functions for cc-peptidases (18, 25, 52, 53). Although structural and experimental evidence strongly suggests a binuclear metallic water activation mechanism at play as the most efficient strategy for this family, the absence of metal 2 (M2) in the BsLcar structure and in those of several homologues (3, 46, 51), together with the activity found with the monometallic BsLcar batch used for crystallization in this work (no extra metal added [see above]), led us to propose an alternative reaction mechanism with only one metal at play. A review of the literature on several homologous enzymes revealed that this topic has already been considered for human aminoacylase 1 (hAcy1) and DapE (36, 46). Alternative mechanisms for mono- and dinuclear metal-containing leucine aminopeptidase (AAP), a cc-peptidase, have also been proved (40). Since it has already been demonstrated that a binuclear metal center is able to hydrolyze a substrate by using a single metal ion (28, 46), we could argue that L-carbamoylases are also able to hydrolyze the carbamoyl moiety of the substrate via the same mechanism: it follows that M1 alone can polarize a water molecule to hydrolyze the scissile amide bond of the substrate, in a manner similar to that proposed previously (28) (see Fig. S4 in the supplemental material). Among the five residues involved in the binuclear metal center in the structures known to date (Table 2), the M2 binding residues (BsLcar Glu^{125} and His^{380}) are totally conserved, whereas M1 binding residues present a higher level of divergence (His^{79} is also fully conserved, but His^{189} may appear as a Glu or Asp residue). This divergence was explained for the homologous EcAam and Skβas enzymes, as a His residue would allow a lower pK_a of the Zn-bound water than that with a negatively charged lateral chain (Glu or Asp) (2, 38). In fact, the His residue would allow an increased nucleophilicity of the attacking hydroxyl, which was hypothesized as necessary to hydrolyze a carbamoyl moiety compared to a peptide bond due to the better resonance stabilization of the ureido group (2, 38). Although the same hypothesis would support a BsLcar mechanism dependent on a single cation (as M1 is coordinated through two His residues, like the case for EcAam and Skβas) (Table 2; see Fig. S4), the proposed mechanism for monometal AAP and DapE depends on a Zn atom coordinated with an aspartate/glutamate and a histidine residue (Asp^{179} and His^{197} or His^{67} and Glu^{163} [46]). This seems to indicate that His replacement might not completely explain an increased nucleophilicity of the water molecule. On the other hand, because Co^{2+} is a harder acid than Zn^{2+}, an electrophilic effect secondary to that produced by the reduced negative charge must be taken into account for BsLcar.

Based on the above, a concomitant effect of both the different metal in BsLcar and the different lateral chain complexing M1 would suggest an enhanced electrophilic effect allowing an alternative reaction mechanism dependent on only one metal atom. As this family of enzymes is known for its substrate promiscuity, we wonder if a flexible bimetallic center (allowing reaction with one or two atoms) would allow a more efficient scavenger amidohydrolase/peptidase activity *in vivo*, regardless of cation availability.

Structural analysis confirms that conserved residues in the dimerization domain are critical for substrate binding. The importance of the His-Asn-Arg triad for substrate binding in L-carbamoylases was shown previously (42). Mutation of counterpart BsLcar residues (Arg^{286}, His^{225}, and Asn^{273}) confirmed their involvement in substrate binding (Table 3). Arg^{286} is located at the end of the third β-strand of the dimerization domain, whereas the other two residues are located on the opposite side of the dimerization domain. However, the dimeric arrangement allows

Downloaded from http://jb.asm.org/ on October 8, 2012 by guest

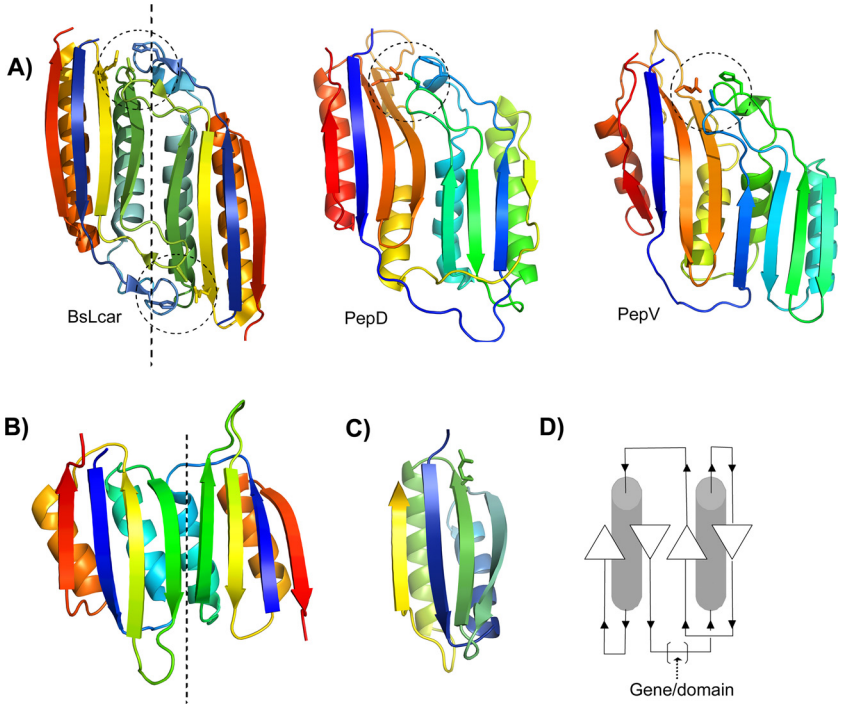

FIG 4 (A) Comparison of the SMBD structures of dimeric BsLcar, monomeric PepD (PDB ID 3MRU), and monomeric PepV (PDB ID 1LFW). Colors represent a spectrum (blue to red) of the order of the secondary elements. The Arg-His-Asn triad is shown as sticks and surrounded by dashed lines. (B) Dimeric arrangement of the ACT domains from D-3-phosphoglycerate dehydrogenase (PDB ID 1YGY) showing similarity to the arrangement of dimeric members of the peptidase M20/M25/M40 family. (C) Stand-alone SMBD belonging to the carboxysome shell protein (PDB ID 2A18), with an Arg residue (sticks) in the same relative position as that for the peptidase M20/M25/M40 family. (D) Topology diagram of the ACT-like domain showing its arrangement and the putative insertion zone where domain fusion would take place.

the formation of a triad composed of Arg^{286} from one monomer and His^{225} and Asn^{273} from the other (Fig. 2). This is further supported by the cacodylate molecule found in the environment of this triad. Asp^{284} is also highly conserved in L-carbamoylases and other members of the peptidase M20/M25/M40 family (such as hAcy1 [41]), and in BsLcar it interacts directly with Arg^{286} through a hydrogen bonding network (Fig. 2). Based on the loss of activity of the D284A mutant and on the similar results obtained for hAcy1 (35), it can be deduced that Asp^{284} plays an essential role in correct positioning of Arg^{286} for substrate binding. We suspect that the partial loss of activity of the T261A mutant was due to partial disruption of the binding network with Arg^{234}; mutation of this Thr was not sufficient to produce changes in BsLcar oligomerization, but it did alter the position of the loop containing His^{225}, as Arg^{234} also seems to anchor/position this structural element (loop containing β8 in Fig. 1B).

Structural analysis of the homologous structures obtained with the Dali server (26) shows a high level of positional conservation of the Arg-His-Asn triad discussed above (Table 2). In fact, the Arg and His residues are strictly conserved. Based on the literature available for homologous enzymes, the conserved Arg residue is or might be necessary for substrate binding in β-alanine synthase (4, 37, 38), EcAam (2), peptidase V (PepV) (31), carnosinase (55), IAA-amino acid hydrolase homolog 2 (ILL2) (7), peptidase D (PepD) (9), DapE (46), hAcy1 (35), peptidase T (PepT) (6, 24), and metallopeptidase (Sapep) (20). Several homologous structures present different molecules bound to these residues, namely, the structures under PDB IDs 1VIX, 1FNO, 3IC1, 3IFE, and 2QYV. On the other hand, the importance of this residue has not been identified for other members of the family, mostly due to the open-and-closed states of these enzymes (49, 51). Taken as a whole, these results reaffirm an essential role of this totally conserved arginine residue in recognition of a carboxyl moiety or analog in the natural substrate for each enzyme of the family.

A new SMBD belonging to the ACT-like superfamily. A Dali search with the isolated BsLcar dimerization and catalytic domains shows greater divergence in the former than in the latter. *Z* values of >20 are found only for Skβas and EcAam, whereas other BsLcar homologues, with *Z* values of >20 for the whole structure (Table 2), show *Z* values in the range of 5 to 15 for the isolated dimerization domain (e.g., PDB IDs 1CG2, 1VIX, 1FNO, 3PFO, and 2ZOG). Sequence similarity in these cases ranges from 10 to 15%. Interestingly, similar *Z* values and sequence similarities were obtained for proteins consisting of this isolated topology, such as carboxysome shell proteins (PDB ID 2A18) (Fig. 4C) (32) or acylphosphatases (PDB ID 2BJE) (12), with sequence similarities as low as 8 to 9%. Further review of the literature concerning these proteins reveals that isolated βαββαβ domains are conserved in a wide variety of enzymes as well as in some transcriptional regulators that are involved in the control of amino acid and purine metabolism and identified as "small-molecule binding domains" (SMBDs) (17). ACT and RAM domains are among the best-studied SMBDs (22), and they constitute a SCOP superfamily known as the ACT/RAM superfamily. These structurally related ferredoxin-like fold proteins mediate allosteric regulation and ligand binding and typically undergo oligomerization through different strat-

Downloaded from http://jb.asm.org/ on October 8, 2012 by guest

egies resulting in different oligomer architectures (14), in some cases similar to that presented by the peptidase M20/M25/M40 family (Fig. 4B) (15, 22). It has also been demonstrated that the sequence divergence of SMBDs such as ACT can expand beyond the detection limits of the sequence-based algorithm of PSI-BLAST (17), which would explain why this is the first time that the ACT-like nature of the dimerization domain of the peptidase M20/M25/M40 family has been found. ACT domains were suggested to present a common ligand binding mode on their discovery (5), whereby the ligand is held in the vicinity of the strand 1-helix 1 interface. This binding mode is partially maintained by means of the conserved His of the peptidase M20/M25/M40 family (and Asn in some cases), also situated in the loop between the counterpart strand and helix. Although ACT (or ACT-like) domains most frequently appear fused at the C- or N-terminal part of the enzymes, they are also known to occur inserted between domains (10, 17), as is the case of the SMBD detected in the peptidase M20/M25/M40 family.

Convergent evolution of peptidase M20/M25/M40 family toward the same binding strategy. Evolution has allowed the presence of proteins with new functions or specificities through domain fusion and recombination and/or differentiation of existing domains (8). The dominant mechanisms accepted to increase protein repertoires are as follows: (i) duplication of DNA sequences coding for one or more domains, (ii) divergence of DNA sequences by mutations, deletions, and/or insertions producing new properties, and (iii) recombination of genes resulting in novel arrangements of domains (11). In this sense, it has already been suggested that β-ureidopropionases and allantoate amidohydrolases most probably evolved by divergent evolution from a common ancestral peptidase (2, 3). A functional convergence after evolutionary divergence has also been proposed for cc-peptidases (39).

Based on the presence of a "double" SMBD for PepV, PepD, and Sapep (PDB IDs 1LFW, 3MRU, and 3KI9, respectively), we aimed to obtain further insights into the probable evolution of this family of enzymes. This "double" SMBD has a different topology depending on the enzyme. Whereas PepD presents a β-(β-α-β-α-β)-α-β-α-β motif, PepV and Sapep present a β-(β-β-α-β-β-α)-α-β-α-β motif. This different arrangement between PepV and PepD (Fig. 4A) and the similarity with the simple dimerization domain of carboxypeptidase G2 (CPG2) were highlighted previously (9, 36). However, a striking characteristic of both the single SMBD (the one presented by BsLcar) and the double SMBD had previously lain partially hidden; the residues involved in the binding of the substrate (Arg-His-Asn) are spatially unaltered in all cases, although in the case of the enzymes with a single SMBD, two domains from different enzyme monomers are required to provide the same amino acids (Fig. 4A).

The common peptidase M20/M25/M40 gene ancestor suggested previously (2, 3) most likely arose by gene insertion (i.e., by chromosome translocation) of an ancestral SMBD-encoding gene into a common ancestor of cc-peptidases (Fig. 5) similar to that proposed by Makarova and Grishin (39). On the other hand, the opposite might also be considered, i.e., that both isolated architectures were created by gene depletion. However, as both cc-peptidases and SMBD proteins are considered primitive proteins (5, 32, 39), gene insertion is a more reliable hypothesis. The PepD, PepV, and Sapep arrangements point toward a later event in evolution, also through domain fusion (Fig. 5), namely, between a

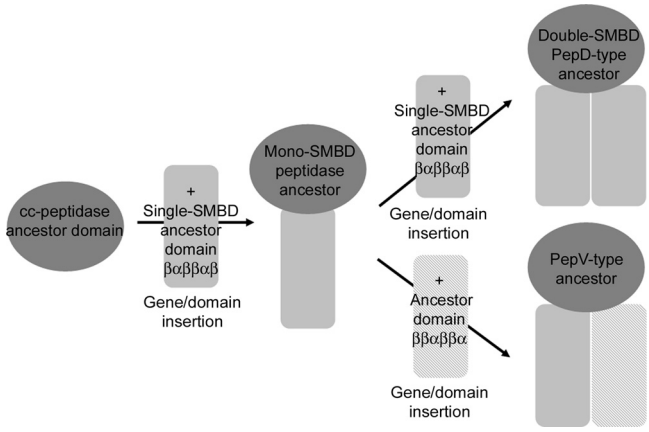

FIG 5 Schematic representation of the putative evolution of the peptidase M20/M25/M40 family through domain insertion of ACT-like domains into an ancient cc-peptidase. Divergent evolution of the mono-SMBD peptidase and double-SMBD PepD-type ancestor and convergent evolution of the PepD-type ancestor are suggested from the structural findings of this work.

β-strand and an α-helix of the dimerization domain (Fig. 4C), allowing the use of the same strategy to cleave different substrates without requiring dimerization. The β-(βαββαβ)-αββαβ topology presented by PepD allows us to infer insertion of a similar SMBD to that presented by the common ancestor of the peptidase family. The conservation of the catalytic triad (Table 2; Fig. 4A) and the similar loops found linking the α and β motifs in BsLcar (Fig. 4A) (containing His and Asn residues from the triad) suggest that this evolution is not synchronic with the insertion of the first SMBD, which does not possess the extended loops (Fig. 4B). This event might therefore have occurred through partial recombination of the existing DNA sequence coding for the SMBD. An alternative explanation would be direct insertion of a duplicated SMBD gene directly into the cc-peptidase ancestor. However, sequence similarity between both βαββαβ domains of PepD is <10%, suggesting insertion of two different SMBD genes. On the other hand, PepV and Sapep topology may have arisen only from insertion of a domain with a ββαββα topology, different from the ACT-type domain, which produced PepD-type peptidases (Fig. 5).

At this stage, what is undeniable from the available experimental information on several members of the peptidase M20/M25/M40 family is the conservation and importance of the Arg-His-Asn triad in mono-SMBD, PepD-type, and PepV-type enzymes. Based on the above data, the common triad arose through a striking case of parallel divergent and convergent evolution in order to cleave the common amide moiety of peptides (by peptidases) and *N*-substituted amino acids (by amidohydrolases), in accordance with previous evolutionary considerations (2, 3, 39).

ACKNOWLEDGMENTS

This work was supported by the European Social Fund (ESF), the European Regional Development Fund (ERDF), the Spanish Ministry of Science and Innovation (projects Factoría Española de Cristalización Consolider-Ingenio 2010 and BIO2010-16800), the Andalusian Regional Council of Innovation, Science and Technology (projects CV7-02651, RNM-5384, and TEP-4691), and the European Science Foundation (COST action CM0701). S.M.-R. was supported by the Andalusian Regional Government, and A.G.-P. was supported by the Fonds Wetenschappelijk Onderzoek (FWO).

Downloaded from http://jb.asm.org/ on October 8, 2012 by guest

We thank Andy Taylor for critical discussion of the manuscript and Pedro Madrid-Romero and Francisco Manuel González-Rico for technical assistance. We also thank Ann Stock for handling the manuscript and the reviewers for their ideas, helpful discussions, and suggestions.

REFERENCES

1. **Afonine PV, Grosse-Kunstleve RW, Adams PD.** 2005. The Phenix refinement framework. CCP4 Newsl. **42**:contribution 8.
2. **Agarwal R, Burley SK, Swaminathan S.** 2007. Structural analysis of a ternary complex of allantoate amidohydrolase from *Escherichia coli* reveals its mechanics. J. Mol. Biol. **368**:450–463.
3. **Andersen B, Lundgren S, Dobritzsch D, Piskur J.** 2008. A recruited protease is involved in catabolism of pyrimidines. J. Mol. Biol. **379**:243–250.
4. **Andújar-Sánchez M, et al.** 2009. Inhibitory effect of different product analogues on β-alanine synthase: a thermodynamic and fluorescence analysis. J. Chem. Ther. **41**:212–220.
5. **Aravind L, Koonin EV.** 1999. Gleaning non-trivial structural, functional and evolutionary information about proteins by iterative database searches. J. Mol. Biol. **287**:1023–1040.
6. **Badger J, et al.** 2005. Structural analysis of a set of proteins resulting from a bacterial genomics project. Proteins **60**:787–796.
7. **Bitto E, et al.** 2009. X-ray structure of ILL2, an auxin-conjugate amidohydrolase from *Arabidopsis thaliana.* Proteins **74**:61–71.
8. **Björklund AK, Ekman D, Light S, Frey-Skött J, Elofsson A.** 2005. Domain rearrangements in protein evolution. J. Mol. Biol. **353**:911–923.
9. **Chang CY, et al.** 2010. Crystal structure and mutational analysis of aminoacylhistidine dipeptidase from *Vibrio alginolyticus* reveal a new architecture of M20 metallopeptidases. J. Biol. Chem. **285**:39500–39510.
10. **Chipman DM, Shaanan B.** 2001. The ACT domain family. Curr. Opin. Struct. Biol. **11**:694–700.
11. **Chothia C, Gough J, Vogel C, Teichmann SA.** 2003. Evolution of the protein repertoire. Science **300**:1701–1703.
12. **Corazza A, et al.** 2006. Structure, conformational stability, and enzymatic properties of acylphosphatase from the hyperthermophile *Sulfolobus solfataricus.* Proteins **62**:64–79.
13. **Davis IW, et al.** 2007. MolProbity: all-atom contacts and structure validation for proteins and nucleic acids. Nucleic Acids Res. **35**:W375–W383.
14. **Devedjiev Y, et al.** 2004. The structure and ligand binding properties of the *B. subtilis* YkoF gene product, a member of a novel family of thiamin/HMP-binding proteins. J. Mol. Biol. **343**:395–406.
15. **Dey S, Grant GA, Sacchettini JC.** 2005. Crystal structure of *Mycobacterium tuberculosis* D-3-phosphoglycerate dehydrogenase: extreme asymmetry in a tetramer of identical subunits. J. Biol. Chem. **280**:14892–14899.
16. **Emsley P, Lohkamp B, Scott WG, Cowtan K.** 2010. Features and development of Coot. Acta Crystallogr. D **66**:486–501.
17. **Ettema TJ, Brinkman AB, Tani TH, Rafferty JB, van der Oost J.** 2002. A novel ligand-binding domain involved in regulation of amino acid metabolism in prokaryotes. J. Biol. Chem. **277**:37464–37468.
18. **Gilboa R, et al.** 2001. Interactions of Streptomyces griseus aminopeptidase with amino acid reaction products and their implications toward a catalytic mechanism. Proteins **44**:490–504.
19. **Gill SC, Von Hippel PH.** 1989. Calculation of protein extinction coefficients from amino acid sequence data. Anal. Biochem. **182**:319–326.
20. **Girish TS, Gopal B.** 2010. Crystal structure of *Staphylococcus aureus* metallopeptidase (Sapep) reveals large domain motions between the manganese-bound and apo-states. J. Biol. Chem. **285**:29406–29415.
21. **Gojkovic Z, Sandrini MPB, Piškur J.** 2001. Eukaryotic beta-alanine synthases are functionally related but have a high degree of structural diversity. Genetics **158**:999–1011.
22. **Grant GA.** 2006. The ACT domain: a small molecule binding domain and its role as a common regulatory element. J. Biol. Chem. **281**:33825–33829.
23. **Guex N, Peitsch MC.** 1997. SWISS-MODEL and the Swiss-PDB ID Viewer: an environment for comparative protein modeling. Electrophoresis **18**:2714–2723.
24. **Håkansson K, Miller CG.** 2002. Structure of peptidase T from *Salmonella typhimurium.* Eur. J. Biochem. **269**:443–450.
25. **Hershcovitz YF, Gilboa R, Reiland V, Shoham G, Shoham Y.** 2007. Catalytic mechanism of SGAP, a double-zinc aminopeptidase from *Streptomyces griseus.* FEBS J. **274**:3864–3876.
26. **Holm L, Rosenström P.** 2010. Dali server: conservation mapping in 3D. Nucleic Acids Res. **38**:W545–W549.
27. **Holz RC, Bzymek KP, Swierczek SI.** 2003. Co-catalytic metallopeptidases as pharmaceutical targets. Curr. Opin. Chem. Biol. **7**:197–206.
28. **Holz RC.** 2002. The aminopeptidase from Aeromonas proteolytica: structure and mechanism of co-catalytic metal centers involved in peptide hydrolysis. Coord. Chem. Rev. **232**:5–26.
29. **Hu HY, Hsu WH, Chien HR.** 2003. Characterization and phylogenetic analysis of a thermostable *N*-carbamoyl-L-amino acid amidohydrolase from *Bacillus kaustophilus* CCRC11223. Arch. Microbiol. **179**:250–257.
30. **Hutchinson EG, Thornton JM.** 1996. PROMOTIF—a program to identify structural motifs in proteins. Protein Sci. **5**:212–220.
31. **Jozic D, et al.** 2002. Crystal structure of the dinuclear zinc aminopeptidase PepV from *Lactobacillus delbrueckii* unravels its preference for dipeptides. Structure **10**:1097–1106.
32. **Kerfeld CA, et al.** 2005. Protein structures forming the shell of primitive bacterial organelles. Science **309**:936–938.
33. **Krissinel E, Henrick K.** 2007. Inference of macromolecular assemblies from crystalline state. J. Mol. Biol. **372**:774–797.
34. **Laskowski RA, Chistyakov VV, Thornton JM.** 2005. PDB ID.sum more: new summaries and analyses of the known 3D structures of proteins and nucleic acids. Nucleic Acids Res. **33**:D266–D268.
35. **Lindner HA, Alary A, Boju LI, Sulea T, Ménard R.** 2005. Roles of dimerization domain residues in binding and catalysis by aminoacylase-1. Biochemistry **44**:15645–15651.
36. **Lindner HA, et al.** 2003. Essential roles of zinc ligation and enzyme dimerization for catalysis in the aminoacylase-1/M20 family. J. Biol. Chem. **278**:44496–44504.
37. **Lundgren S, Andersen B, Piskur J, Dobritzsch D.** 2007. Crystal structures of yeast beta-alanine synthase complexes reveal the mode of substrate binding and large scale domain closure movements. J. Biol. Chem. **282**:36037–36047.
38. **Lundgren S, Gojkovic Z, Piškur J, Dobritzsch D.** 2003. Yeast β-alanine synthase shares a structural scaffold and origin with dizinc-dependent exopeptidases. J. Biol. Chem. **278**:51851–51862.
39. **Makarova KS, Grishin NV.** 1999. The Zn-peptidase superfamily: functional convergence after evolutionary divergence. J. Mol. Biol. **292**:11–17.
40. **Martínez-Gómez AI, et al.** 2011. *N*-Carbamoyl-β-alanine amidohydrolase from *Agrobacterium tumefaciens* C58: a promiscuous enzyme for the production of amino acids. J. Chromatogr. B Analyt. Technol. Biomed. Life Sci. **879**:3277–3282.
41. **Martínez-Gómez AI, et al.** 2009. Potential application of *N*-carbamoyl-beta-alanine amidohydrolase from *Agrobacterium tumefaciens* C58 for beta-amino acid production. Appl. Environ. Microbiol. **75**:514–520.
42. **Martínez-Rodríguez S, et al.** 2006. Thermodynamic and mutational studies of L-*N*-carbamoylase from *Sinorhizobium meliloti* CECT 4114 catalytic centre. Biochimie **88**:837–847.
43. **Martínez-Rodríguez S, et al.** 2008. Crystallization and preliminary crystallographic studies of the recombinant L-*N*-carbamoylase from *Geobacillus stearothermophilus* CECT43. Acta Crystallogr. Sect. F Struct. Biol. Cryst. Commun. **64**:1135–1138.
44. **Martínez-Rodríguez S, Martínez-Gómez AI, Rodríguez-Vico F, Clemente-Jiménez JM, Las Heras-Vázquez FJ.** 2010. Carbamoylases: characteristics and applications in biotechnological processes. Appl. Microbiol. Biotechnol. **85**:441–458.
45. **Murshudov GN, et al.** 2011. REFMAC5 for the refinement of macromolecular crystal structures. Acta Crystallogr. D Biol. Crystallogr. **67**:355–367.
46. **Nocek BP, Gillner DM, Fan Y, Holz RC, Joachimiak A.** 2010. Structural basis for catalysis by the mono- and dimetalated forms of the dapE-encoded *N*-succinyl-L,L-diaminopimelic acid desuccinylase. J. Mol. Biol. **397**:617–626.
47. **Ogawa J, Shimizu S.** 1994. Beta-ureidopropionase with *N*-carbamoyl-alpha-L-amino acid amidohydrolase activity from an aerobic bacterium, Pseudomonas putida IFO 12996. Eur. J. Biochem. **223**:625–630.
48. **Pozo-Dengra J, et al.** 2010. Evaluation of substrate promiscuity of an L-carbamoyl amino acid amidohydrolase from *Geobacillus stearothermophilus* CECT43. Biotechnol. Prog. **26**:954–959.
49. **Rowsell S, et al.** 1997. Crystal structure of carboxypeptidase G2, a bacterial enzyme with applications in cancer therapy. Structure **5**:337–347.
50. **Säbel CE, Shepherd JL, Siemann S.** 2009. A direct spectrophotometric method for the simultaneous determination of zinc and cobalt in met-

Downloaded from http://jb.asm.org/ on October 8, 2012 by guest

alloproteins using 4-(2-pyridylazo)resorcinol. Anal. Biochem. **391**: 74–76.
51. **Shi D, Yu X, Roth L, Tuchman M, Allewell NM.** 2007. Structure of a novel *N*-acetyl-L-citrulline deacetylase from *Xanthomonas campestris*. Biophys. Chem. **126**:86–93.
52. **Stamper C, et al.** 2001. Inhibition of the aminopeptidase from Aeromonas proteolytica by L-leucinephosphonic acid. Spectroscopic and crystallographic characterization of the transition state of peptide hydrolysis. Biochemistry **40**:7035–7046.
53. **Sträter N, Lipscomb WN.** 1995. Two-metal ion mechanism of bovine lens leucine aminopeptidase: active site solvent structure and binding mode of L-leucinal, a gem-diolate transition state analogue, by X-ray crystallography. Biochemistry **34**:14792–14800.
54. **Stumpp T, Wilms B, Altenbuchner J.** 2000. Ein neues L-rhamnose-induzierbares expressionssystem für *Escherichia coli*. Biospektrum **6**:33–36.
55. **Unno H, et al.** 2008. Structural basis for substrate recognition and hydrolysis by mouse carnosinase CN2. J. Biol. Chem. **283**:27289–27299.
56. **Vagin A, Teplyakov A.** 1997. MOLREP: an automated program for molecular replacement. J. Appl. Crystallogr. **30**:1022–1025.
57. **Wyatt PJ.** 1993. Light scattering and the absolute characterization of macromolecules. Anal. Chim. Acta **272**:1–40.

Downloaded from http://jb.asm.org/ on October 8, 2012 by guest